PERGAMON

International Journal of Heat and Mass Transfer 44 (2001) 2137–2146

International Journal of HEAT and MASS TRANSFER

www.elsevier.com/locate/ijhmt

# Study of a laminar falling film flowing over a wavy wall column: Part I. Numerical investigation of the flow pattern and the coupled heat and mass transfer

S. Negny, M. Meyer *, M. Prevost

*UMR 5503 INP-ENSIGC/CNRS Groupe Séparation Gaze–Liquide, 18 Chemin de la Loge, 31078 Toulouse Cedex 04, France*

Received 26 September 1998; received in revised form 31 May 2000

**Abstract**

Flow pattern and heat and mass transfer characteristics for a film flowing over a vertical wavy column are numerically investigated in a laminar flow regime. In our approach, the heat and mass transfer coefficients are avoided in order to include hydrodynamics directly in the heat and mass transfer rates. As a consequence the numerical model is decomposed into two steps. Firstly, the flow pattern for a film with a free interface is developed. Secondly, heat and mass transfer are investigated with the incorporation of velocity fields. The heat and mass transfer coefficients increase in laminar flow. 

## 1. Introduction

Heat and mass transfer enhancement, coupled with desire to decrease apparatus size is one of the principal axes of research in chemical engineering. Corrugated surfaces, more specifically, wavy walled surfaces are a way for solving this industrial requirement. This kind of wall is employed in compact heat exchangers for the purpose of enhancing the rate of heat transfer. Another thermal use of the wavy surfaces (but not in the case of films) is the dissipation of heat within electronic circuits, as the component performance and reliability are strongly dependent on operating temperature. Wavy walls are employed in medical operations, too, in order to increase mass transfer (blood oxygenator).

As a consequence, numerical and experimental studies on channels with wavy walls arise from the above applications. Nishimura et al. [1–4] have published several reports on the flow structure and mass transfer rate in a wavy channel. Their research widely covers steady flow. Hydrodynamic characteristics, i.e., flow patterns, friction factor, wall shear stress, were investigated for laminar, transitional and turbulent flow regimes. These investigations were numerically realised using a finite element method and experimentally by flow visualisation (hydrogen bubble method). There was good agreement between the theoretical and experimental results: the laminar flow ($Re < 350$) showed a two-dimensional steady vortex in the furrows but the turbulent flow showed a three-dimensional unsteady vortex (unsteady flow in the spanwise direction). The relationship between the flow pattern and mass transfer was established for all regimes. An electrochemical method was used for validating the theoretical model. The local Sherwood number distributions showed a large variation when the recirculation zone appeared. In the laminar flow range, the wavy channel did not increase the mass transfer, however, in the turbulent flow range the increase was important.

Sparrow et al. [5,6] experimentally studied the geometrical effects on the heat transfer coefficient in wavy walled channels. First, the effect of interwall spacing was investigated. When the interwall spacing tended to increase the recirculation zone became more important. Therefore, the Nusselt number increased appreciably (30% in the interwall spacing range considered). However, the friction factor underwent a greater increase

* Corresponding author.
*E-mail address:* michel.meyer@ensigct.fr (M. Meyer).

0017-9310/01/$ - see front matter 
PII: S0017-9310(00)00236-2

**Nomenclature**

| | |
|---|---|
| $a$ | wave amplitude (m) |
| $C$ | concentration (mol/m$^3$) |
| $C^*$ | equilibrium concentration (mol/m$^3$) |
| $C_m$ | mean concentration (mol/m$^3$) |
| $D$ | diffusion coefficient (m$^2$/s) |
| $D_m$ | mean diameter (m) |
| $D_p$ | wall diameter (m) |
| $f_i$ | function $i$ |
| $F$ | vector of function |
| $g$ | gravitational acceleration (m$^2$/s) |
| $h_{ci}$ | interfacial mass transfer coefficient for the wavy tube (m/s) |
| $h^0_{ci}$ | interfacial mass transfer coefficient for the smooth tube (m/s) |
| $h_{tp}$ | wall heat transfer coefficient (W/(m$^2$ K)) |
| $H$ | molar enthalpy (J/mol) |
| $J(x)$ | Jacobian matrix |
| $k$ | iteration |
| $L_k$ | submatrix of $J$ |
| $M_k$ | submatrix of $J$ |
| $n$ | normal to the interface |
| $N_k$ | submatrix of $J$ |
| $N_r$ | radial mass transfer rate (mol/(m$^2$ s)) |
| $Nu$ | mean Nusselt number for wavy tube |
| $Nul$ | local Nusselt number for wavy tube $Nul = h_{tp}D_p/\lambda$ |
| $Nu0$ | Nusselt number for smooth tube $Nu0 = h^0_{tp}D_m/\lambda$ |
| $N_z$ | axial mass transfer rate (mol/(m$^2$ s)) |
| $p$ | wavelength (m) |
| $P$ | pressure (Pa) |
| $P_0$ | gas pressure (Pa) |
| $q_r$ | radial heat transfer (J/(m$^2$ s)) |
| $q_z$ | axial heat transfer (J/(m$^2$ s)) |
| $Q_l$ | volumetric flow (m$^3$/s) |
| $r$ | radial component (m) |
| $r_i$ | interfacial radius (m) |
| $r_m$ | mean radius (m) |
| $r_p$ | wall radius (m) |
| $Re$ | Reynolds number $Re = 4\Gamma/\mu$ |
| $Re_2$ | Reynolds number for the correlation $Re_2 = 4Q_l\rho/(\mu D_m\pi)$ |
| $Sc$ | Schmidt number $Sc = \mu/(D\rho)$ |
| $Sh$ | mean Sherwood number for wavy tube |
| $Shl$ | local Sherwood number for wavy tube $Shl = h_{ci}D_p/D$ |
| $Sh0$ | Sherwood number for smooth tube $Sh0 = h^0_{ci}D_m/D$ |
| $T$ | temperature (K) |
| $T_g$ | gas temperature (K) |
| $T_i$ | interfacial temperature (K) |
| $T_m$ | mean temperature (K) |
| $T_p$ | wall temperature (K) |
| $t$ | tangent to the interface |
| $v_r$ | radial velocity (m/s) |
| $v_t$ | tangential velocity (m/s) |
| $v_z$ | axial velocity (m/s) |
| $x$ | vector of variables |
| $x_i$ | variable $i$ |
| $z$ | axial component (m) |

*Greek symbols*

| | |
|---|---|
| $\alpha$ | angle between the tangent of the interface and the horizontal (rad) |
| $\delta$ | film thickness (m) |
| $\delta^*$ | non-dimensional film thickness $\delta^* = \delta/p$ |
| $\psi$ | stream function |
| $\omega$ | vorticity |
| $\xi$ | axial component in the mathematical domain |
| $\eta$ | radial component in the mathematical domain |
| $\sigma$ | surface tension (N/m) |
| $\nu$ | dynamic viscosity |
| $\lambda$ | heat conduction coefficient (J/(m s K)) |
| $\Gamma$ | mass flow rate divided by the wetted perimeter (kg/(m$^2$ s)) |
| $\rho$ | liquid density (kg/m$^3$) |
| $\mu$ | liquid viscosity (Pa s) |

*Mathematical operator*

$\nabla^2 = \frac{\partial^2}{\partial r^2} - \frac{1}{r}\frac{\partial}{\partial r} + \frac{\partial^2}{\partial z^2}$

(over twofold). Secondly, experiments were performed to determine the effect of the wall peak radius of curvature on the heat transfer coefficient and friction factor (comparisons with sharp peak corrugated channel). For a given Reynolds number the greater the radius of curvature of the peak, the more the Nusselt number decreases. The friction factor has the same variation as the Nusselt number but in a sharper manner. This phenomenon was emphasised with the increase in Reynolds number. In the two papers, comparisons were carried out under different types of constraints: fixed mass flow rate, fixed pumping power, fixed pressure drop.

The wavy walled channels were studied numerically and experimentally by several other authors [7–12] because they appeared to allow for the increase of heat transfer rate in exchangers. This is attributed to the recirculation zone which appears in the furrows. The difficulty is that the fluid has to follow the wall curvature creates a vortex which increases the heat transfer rate by the renewal of the thermal boundary layer (for high enough Reynolds numbers).

The above relates to the flow in full channels or tubes. Apparently no work on our research preoccupation has yet been reported in the literature. The increase of heat and mass transfer appears to be interesting for gas–liquid contactors. The following presentation approaches the case of a falling film flowing inside a vertical wavy walled tube. Firstly, modelisation of the hydrodynamics of the film is necessary in order to include the velocity fields in the determination of simultaneous heat and mass transfer rates. The particularity of this model is that it contains a free gas–liquid interface. The gas phase is supposed to be stagnant, i.e., no gas flow in this phase. Secondly, this time the simultaneous heat and mass transfer are simulated. The last two parts of this paper are related to the model's resolution and results of the simulations.

## 2. Modelisation

All the calculations presented in this paper were performed for symmetrical tubes with a sinusoidal wavy wall. The geometry and the different geometrical parameters are presented in Fig. 1. As the wall is sinusoidal its shape is supposed to follow the equation:

$$r_p = r_m + a\cos\left(\frac{2\pi z}{p}\right). \tag{1}$$

The theoretical model can be decomposed into two parts. The former concerns the solution of the hydrodynamics of the film with a free interface flowing over a wavy tube. The latter studies the coupled heat and mass transfer. The velocity fields link the two parts, i.e., it is a result of the first part and is introduced into the second part in order to evaluate the transfer rates.

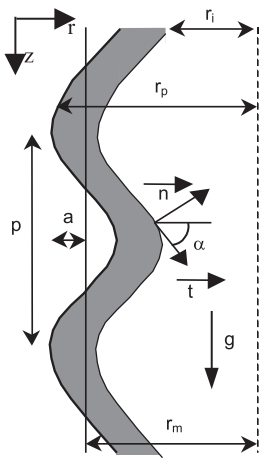


Fig. 1. Geometry of the sinusoidal wavy tube.

### 2.1. First part: hydrodynamic modelisation

The theoretical investigation is carried out by using Naviers–Stokes equations for the film and a specific equation for the interface position. In the present study, the flow is considered to be axisymmetric ($r$, $z$ components) with no variation in the spanwise direction. A newtonian, incompressible, isothermal film flows down the inside of the vertical wavy tube. All the fluid properties are kept constant. The Naviers–Stokes equations are used. For laminar flow with constant properties the differential equations may be simplified by formulation in terms of stream function $\psi$. The velocity components are expressed as derivatives of $\psi$

$$v_z = -\frac{1}{r}\frac{\partial\psi}{\partial r}, \quad v_r = \frac{1}{r}\frac{\partial\psi}{\partial z}. \tag{2}$$

In such a way, the equation of continuity is automatically satisfied. The two non-vanishing components of the equation of motion can be combined to eliminate the terms of pressure and gravity. Even though these two terms are not directly introduced into the equations they are taken into account. This procedure leads to a fourth-order scalar equation in terms of $\psi$. The vorticity is introduced in order to decrease the order of the differential equation

$$\omega = \nabla^2\psi. \tag{3}$$

By this substitution, the system is composed of two second-order equations instead of one fourth-order equation. For numerical resolution it is more reasonable to have two second-order equations.

The two-dimensional Naviers–Stokes equations expressed in terms of vorticity and stream functions are

$$-\frac{1}{r}\left(\frac{\partial\psi}{\partial r}\frac{\partial\omega}{\partial z}-\frac{\partial\psi}{\partial z}\frac{\partial\omega}{\partial r}\right)-\frac{2}{r^2}\frac{\partial\psi}{\partial z}\omega = \nu\left(\frac{\partial^2\omega}{\partial r^2}-\frac{1}{r}\frac{\partial\omega}{\partial r}+\frac{\partial^2\omega}{\partial z^2}\right),$$
$$\omega = \frac{\partial^2\psi}{\partial r^2}-\frac{1}{r}\frac{\partial\psi}{\partial r}+\frac{\partial^2\psi}{\partial z^2}. \tag{4}$$

It is interesting to note the physical significance of streamlines: lines of constant $\psi$. In steady flow, streamlines represent particle trajectories within the fluid.

The interface position is described by a specific equation based on a force balance, and it takes into account the shape effects. For the statement of this equation we made several assumptions: constant surface tension (i.e., no surfactant), no ripples on the interface, constant gas pressure, no viscous effects in the gas phase. For more details on the formulation and the statement of this equation refer to [13]

$$\frac{\partial^2 r_i}{\partial z^2}-\frac{1}{\sigma}(P-P_0)-\frac{1}{r_i}=0. \tag{5}$$

The term $P$ is not easily accessible. The only equation in which the pressure appears is in the $z$ projection of the Naviers–Stokes equations, written in terms of velocity. In fact, it is the term $dP/dz$ which appears. To calculate $P$, the $z$ projection of the equation must be integrated but there is no boundary condition for $P$. This way to proceed is not satisfactory. Another way to avoid this problem is to derive Eq. (5), so that the term $dP/dz$ appears and it is evaluated by the $z$ projection in which the term of gravity appears

$$r_i^2\left(\frac{d^3 r_i}{dz^3}-\frac{1}{\sigma}\frac{\partial P}{\partial z}\right)+\frac{dr_i}{dz}=0. \tag{6}$$

Eqs. (4) and (6) are non-dimensionalised with respect to the wavelength ($p$) and the volumetric flow ($Q_l$).

*2.1.1. Boundary conditions*

At the wall no slip conditions are used between the liquid and the solid surface. The periodical repetition of the wave shape, as the wavy wall is supposed to be sinusoidal, inspires periodical conditions for the velocity and they are translated in terms of stream function and vorticity in (10).

Further, the continuity of the tangential velocity across the interface is translated as follows, as the gas phase is stagnant, there is no tangential velocity in this phase (Fig. 1):

$$\frac{\partial v_t}{\partial n}=0, \tag{7}$$

$$\begin{aligned}\frac{\partial v_t}{\partial n}={}& C1\frac{\partial v_r}{\partial r}-A1\frac{\partial v_z}{\partial r}+B1\frac{\partial v_r}{\partial z}-C1\frac{\partial v_z}{\partial z}\\ &-(C1v_r+B1v_z)\frac{d\alpha}{dz}\quad\left(A1=\sin^2\alpha,\right.\\ &\left.B1=\cos^2\alpha,\quad C1=\sin\alpha\cos\alpha\right).\end{aligned} \tag{8}$$

Expressed in terms of stream function

$$\begin{aligned}\frac{\partial v_t}{\partial n}={}&\frac{1}{r}\left\{\left(B1\frac{d\alpha}{dz}-\frac{A1}{r}\right)\frac{\partial\psi}{\partial r}-C1\left(\frac{1}{r}+\frac{d\alpha}{dz}\right)\frac{\partial\psi}{\partial z}\right.\\ &\left.+A1\frac{\partial^2\psi}{\partial r^2}+B1\frac{\partial^2\psi}{\partial z^2}+2C1\frac{\partial^2\psi}{\partial r\partial z}\right\},\end{aligned} \tag{9}$$

$$\begin{aligned}&\psi(r,0)=\psi(r,1)\quad\forall r\in[r_i,r_p],\\ &\omega(r,0)=\omega(r,1)\quad\forall r\in[r_i,r_p],\\ &\frac{\partial\psi}{\partial z}(r,0)=\frac{\partial\psi}{\partial z}(r,1)\quad\forall r\in[r_i,r_p].\end{aligned} \tag{10}$$

The mathematical translation, for the interface reaching a minimum at the beginning and the end of each wave, gives boundary conditions for (6). Eqs. (4) and (6) describe the hydrodynamics of the film with a free interface flowing over a wavy surface. This model gives the velocity fields and the film thickness, which are included in the heat and mass transfer model.

*2.2. Second part: heat and mass transfer modelisation*

The model is established for the absorption of a gas ($CO_2$) by a wavy film of liquid ($H_2O$). In this paper, the modelisation for two components is presented. However, it can be extended to a multicomponent absorption. The heat and mass transfer are coupled and hydrodynamics are introduced into the transfer rates, by the velocity field, as follows:

$$N_i=v_iC-D\frac{\partial C}{\partial i},\quad i=r,z, \tag{11}$$

$$q_i=-\lambda\frac{\partial T}{\partial i}+\sum_j N_i^j H^j,\quad j=1,2. \tag{12}$$

As for the mass transfer, the axial diffusion is neglected with respect to convection. The same assumption is made for the axial heat conduction in the case of heat transfer. For the transfer of two components, the thermal conduction coefficient, the diffusion coefficient and the enthalpy are supposed to be dependent on temperature and composition (in the multicomponent case the diffusion coefficient is supposed to be independent of the composition because we have no means to evaluate $D_{j,m}$). With these dependencies, the quantities are evaluated at each node of the grid. The thermal conduction of the mixture is evaluated by the correlation of Vredeveld [14]. The diffusion coefficient is evaluated by the Tyn and Calus correlation and Vignes law [15]. Before its use, the correlation was tested and compared with results found in the literature, Table 1. For our case of application: absorption of $CO_2$ by water the evaluation of the diffusion coefficient is acceptable.

The enthalpy is calculated by the use of a thermodynamic software package Prophy [19]. Prophy is a general software package which widely covers the thermodynamic properties, of a component or a mixture, for various thermodynamic models. Prophy is connected to the DIPPR library which contains the properties of approximately two thousand components.

For the moment, the system is composed of four (Eqs. (11) and (12) according to $r$ and $z$) with six variables: $N_r$, $N_z$, $q_r$, $q_z$, $C$ and $T$. In order to obtain a

Table 1
Comparison of the calculated diffusion coefficient

| Solute | Solvent | Percent error (%) | Ref. |
|---|---|---|---|
| Water | Acetone | 6.9 | [16] |
| Water | Ethanol | 3.4 | [17] |
| Carbon dioxide | Water | 1.9 | [18] |

consistent system, we have added two additional equations relative to heat and mass transfer rate balances, which are

$$N_r = v_r C - D\frac{\partial C}{\partial r}, \quad N_z = v_z C,$$
$$q_r = -\lambda\frac{\partial T}{\partial r} + \sum_j N_r^j H^j,$$
$$q_z = \sum_j N_z^j H^j, \quad \frac{\partial N_z}{\partial z} + \frac{\partial N_r}{\partial r} + \frac{1}{r}N_r = 0,$$
$$\frac{\partial q_z}{\partial z} + \frac{\partial q_r}{\partial r} + \frac{1}{r}q_r = 0. \tag{13}$$

*2.2.1. Boundary conditions*

*2.2.1.1. At the interface*. At the interface, equilibrium is reached between the two phases. As the gas phase is supposed to be stagnant its temperature is constant.

$$r = r_\mathrm{i}, \quad q_r = h(T_\mathrm{g} - T_\mathrm{i}), \quad C = C^*(T_\mathrm{i}). \tag{14}$$

*2.2.1.2. At the wall*. The temperature of the wall is kept constant throughout all the simulations. The wall is a solid surface so there is no mass transfer through it

$$r = r_\mathrm{p}, \quad T = T_\mathrm{p}, \quad N_r = 0. \tag{15}$$

*2.2.1.3. At the entrance*. The concentration of all species is supposed to be known at the entrance of the wave, so all the mass transfer flows are determined because the velocity field is given (result of the hydrodynamic model). For the heat transfer, the entrance temperature is supposed to be known and then the enthalpy can be evaluated for all species. As we know the mass transfer flows and the enthalpy of all species the heat flow at the entrance is determined

$$z = 0, \quad N_z^i = v_z C^{i0} = N_z^{i0},$$
$$z = 0, \quad q_z = \sum_i N_z^{i0} H^{i0} = q_0. \tag{16}$$

The two models concerning hydrodynamics and heat and mass transfer have been presented above, and their resolution is now presented.

*2.3. Resolution*

To solve both systems, a discretisation appears to be necessary but it is impossible to do so within the physical domain. The complexity of our domain of calculation, caused by the wall waviness, does not allow us to use a classic finite difference scheme because of the non-orthogonal co-ordinates. So, an algebraic transformation, suggested by Panday [20] is used in order to transform the physical domain into a mathematical one which contains rectangular co-ordinates (Fig. 2).

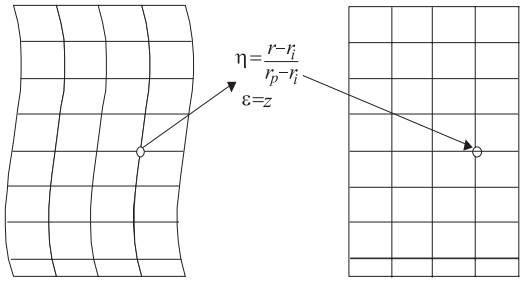


Fig. 2. Transformation of the physical domain.

All the equations and boundary conditions of the two models are transformed in the mathematical domain by using the following derivatives:

$$\left(\frac{\partial}{\partial r}\right)_z = \frac{\partial \eta}{\partial r}\left(\frac{\partial}{\partial \eta}\right)_\xi,$$
$$\left(\frac{\partial^2}{\partial r^2}\right)_z = \left(\frac{\partial \eta}{\partial r}\right)^2\left(\frac{\partial^2}{\partial \eta^2}\right)_\xi,$$
$$\left(\frac{\partial}{\partial z}\right)_r = \left(\frac{\partial}{\partial \xi}\right)_\eta + \frac{\partial \eta}{\partial z}\left(\frac{\partial}{\partial \eta}\right)_\xi,$$
$$\left(\frac{\partial^2}{\partial z^2}\right)_r = \left(\frac{\partial^2}{\partial \xi^2}\right)_\eta + \frac{\partial^2 \eta}{\partial z^2}\left(\frac{\partial}{\partial \eta}\right)_\xi + 2\frac{\partial \eta}{\partial z}\frac{\partial^2}{\partial \eta \partial \xi} + \left(\frac{\partial \eta}{\partial z}\right)^2\left(\frac{\partial^2}{\partial \eta^2}\right)_\xi. \tag{17}$$

In order to solve the equations of the two systems, they require a finite difference method to evaluate the derivatives. In the mathematical domain, the partial derivatives are approximated by using a second-order central finite difference formula. The discretisation in both directions leads to two systems of algebraic non-linear equations. For the hydrodynamics, at each node of the grid, vorticity and stream functions are calculated and we have added an extra variable, the interfacial radius, to each node of the interface. For heat and mass transfer, the grid computation is the same as for the hydrodynamics because the velocity field is included in the model. A $80 \times 60$ grid ($z \times r$) is well adapted because the results are precise enough and the CPU time cost is acceptable for a tube with the following geometrical characteristics: $p = 21.5$ mm and $a = 3$ mm. For a wider grid $60 \times 40$ the results between this grid and the $80 \times 60$ one differ by more than 3%, and at the same time the CPU time increases from 1 to 3 h. On the other hand, a refined grid $100 \times 80$ gives a difference in results of about 1% with respect to the $80 \times 60$ grid, but the CPU time is greatly increased: 9 h of calculation time are needed. All calculations are realised on an IBM RS 6000 390. In the second model, the temperature, concentration, heat and mass transfer rates in both directions are calculated at each node of the grid.

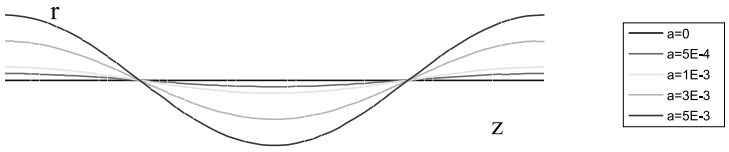


Fig. 3. Variation of the wave shape with the amplitude.

For both the models, we have chosen a global method of resolution, i.e., all equations of each model are solved simultaneously. As the discretisation leads to non-linear system, an iterative Newton (Appendix A) method seems to be well adapted to our problem. For both cases, the Jacobian matrices are evaluated analytically, and a judicious arrangement of the terms gives a three-diagonal block matrix structure. This particular sparce structure (Appendix A) is exploited during the resolution in order to decrease CPU time and to reduce calculation error. This method has an inconvenience, initialisation. Our way of initialising is to use our physical knowledge of the problem. Indeed, the results of the film flowing over a smooth tube are used for a fixed Reynolds number. For the hydrodynamics the wave amplitude is used as a homotopic parameter. Therefore, the wave amplitude increases gradually (Fig. 3), and when the results for a wave amplitude are obtained we initialise the simulation for the next wave amplitude with these results.

## 3. Results and discussion

The first step is to validate the models, and for this a particular case has been selected and solved: a falling film flowing inside a smooth wall column. With the same assumption of no ripples on the interface, an analytical solution of the velocity fields and the film thickness is possible for the case of a falling film flowing over a smooth surface. The calculated film thickness of the model differs only by 0.5% from the analytical results. Concerning the velocity field the error is in the same order of magnitude. In consequence the semi-parabolic Nusselt profile for the velocity field and film thickness is in agreement with analytical results. Fig. 4 represents the comparison of the calculated mass transfer coefficient for the smooth column with that given by [23] (correlation (18)). After testing the models the simulation of the vertical wavy walled tube can begin.

### 3.1. Hydrodynamic results

All hydrodynamic results are explained in a previous publication [21]. In this part, we briefly remind the principal hydrodynamic results in order to understand in detail the influence of hydrodynamics on the transfers. Fig. 5 represents the calculated streamlines for various Reynolds numbers. For $Re = 1$ (Fig. 5(a)) the streamlines are symmetrical around the maximum cross-section of the tube and follow the wall shape. At $Re = 15$ (Fig. 5(b)) the recirculation zone appears in the valleys of the tube. The recirculation zone can be characterised by two important points. The first, encountered in the way of the flow, is the separation point. At this location the fluid is unable to follow the wall curvature and therefore it separates from the wall. The second point is the spot where the flow reattaches to the wall: reattachment point. The vortex extends

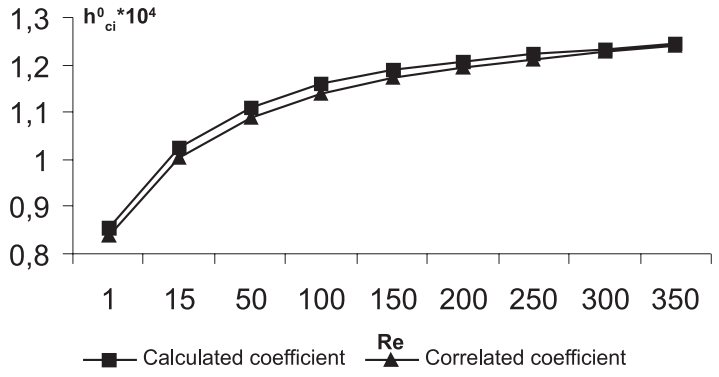


Fig. 4. Comparison of the mass transfer coefficients.

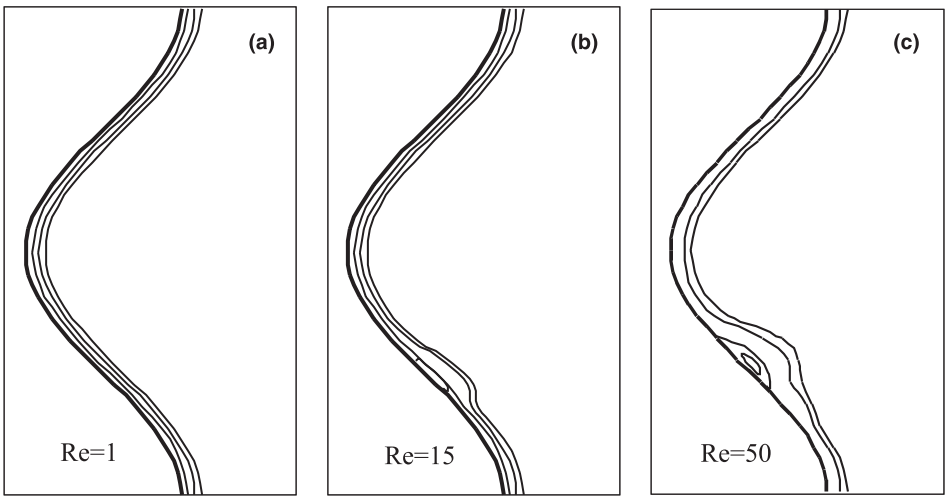


Fig. 5. Streamlines for various *Re*.

between these two points and a reverse flow appears near the wall. In the optimum case, the total recirculation zone does not exceed 70% of the film thickness, which is very important for the transfer rate at the interface. The vortex arises slightly upstream from the maximum cross-section. In increasing the Reynolds number (Fig. 5(c)) the vortex becomes more consistent in size and in strength. Its centre shifts downstream. This tendency is kept until the flow becomes turbulent, i.e., $Re = 350$. As in the case of the flow in a full channel, presented above, a part of the main flow passes on the recirculation zone. This part tends to narrow down with an increasing Reynolds number. The same phenomenon is observed by Nishimura et al. [2]. In the case of a falling film flowing over a vertical wavy tube the inertial effects shift the vortex centre further downstream.

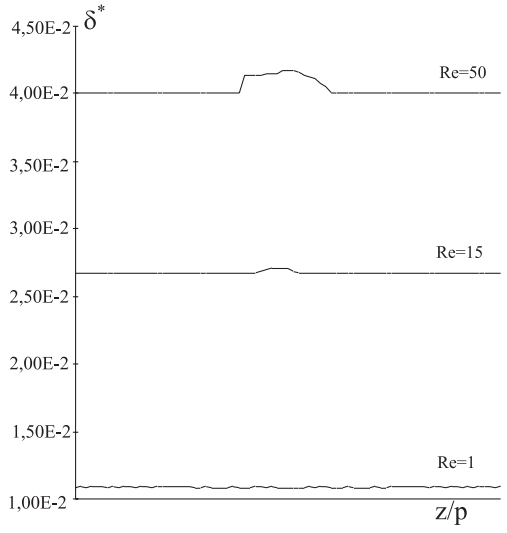


Fig. 6. Non-dimensional film thickness $\delta^*$.

The vortex location plays an important role in the thickness of the film. As already mentioned before, the interface is free and so in Fig. 6 the non-dimensional film thickness is represented. The film thickness is constant along one wave until $Re = 15$, i.e., the recirculation zone arises. After $Re = 15$, the film thickness grows up in the furrows, more precisely at the location of the recirculation zone. The back mixing phenomenon increases the film thickness. The maximum thickness occurs at the vortex centre so the maximum shifts downstream as the Reynolds number increases (as the vortex centre). The more the Reynolds number is incremented the more the vortex is intensified and the thicker the film becomes.

In Fig. 7, the wall shear stress is plotted against the position on the wave for various Reynolds numbers. For $Re = 1$ the wall shear stress has a positive value and is symmetrical with regard to the maximum cross-section (medium of the cell). When the recirculation zone arises, the reverse flow generates negative values included between the separation and reattachment points. Near the separation point there is the location of a local minimum and a minimum rises just before the reattachment point. The value of this minimum decreases when the Reynolds number increases. An explanation for this is that the vortex progresses rapidly at the separation point and it narrows slowly to a limit form at the reattachment point. The presence of the minimum and the maximum shows that there is a particular local flow at the separation and reattachment points. The same results were found by Sobey [22].

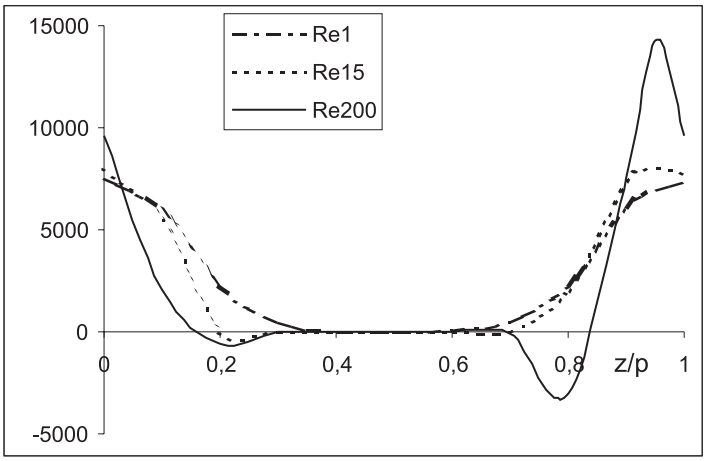


Fig. 7. Non-dimensional wall shear stress.

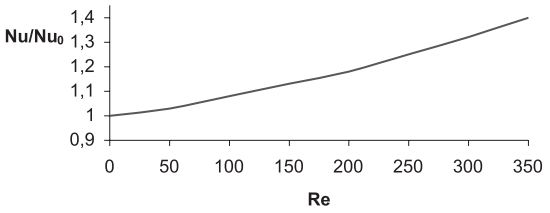


Fig. 8. Comparison of the global Nusselt numbers.

### 3.2. Heat and mass transfer results

The purpose is to compare the performance of the wavy surface with regard to the smooth surface. Both surfaces are compared in terms of transfer coefficients calculated for the same column length. Correlation found in the literature [23] is used to evaluate the heat and mass transfer coefficients for the smooth tube.

$$h_{ci}^{0} = 4.588 \times 10^{-3} Re_2^{0.5513} Sc^{1/2} D. \tag{18}$$

The heat transfer comparison is established by the calculation of the Nusselt number at the wall. For the mass transfer, the Sherwood number is used at the interface. For the wavy surface the local heat and mass transfer coefficients are calculated by the following expressions:

$$h_{tp} = q_r(r_p)/(T_p - T_m), \tag{19}$$

$$h_{ci} = N_r(r_i)/(C^* - C_m) \tag{20}$$

with

$$T_m = \frac{\int_{r_p}^{r_i} v_z T \, dr}{\int_{r_p}^{r_i} v_z \, dr}, \tag{21}$$

$$C_m = \frac{\int_{r_p}^{r_i} v_z C \, dr}{\int_{r_p}^{r_i} v_z \, dr}. \tag{22}$$

The mean temperature $T_m$, is the temperature which would be measured if the tube were cut at $z$ and if the fluid issuing were collected in a container and thoroughly mixed (this temperature is sometimes referred to as the *flow average temperature*). The same explanation is possible for the mean concentration. A comparison of the mean Nusselt numbers at the wall is represented in Fig. 8. The mean Nusselt and Sherwood numbers are calculated by the following expressions:

$$Nu = \frac{\int_0^p Nul \, dz}{p}, \quad Sh = \frac{\int_0^p Shl \, dz}{p}. \tag{23}$$

For the same projected area, the mean Nusselt number for the wavy surface is greater than the Nusselt number of the smooth surface. The more the Reynolds number increases the more the difference is enlarged. If the comparison is established for the same column area the wavy surface does not increase the Nusselt number, except when the recirculation zone appears. As the increasing Reynolds number enlarges the ratio (even for the same column area) the intensity of the recirculation zone affects the heat transfer coefficient. When *Re* increases, the size and the strength of the vortex evolve in the same way, so the renewal of the thermal boundary layer, by the reverse flow, is more intense. It can be underlined that the increase is not important in the case of laminar flow.

Let us examine the local heat transfer in order to understand the increase of the wavy wall with regard to the smooth one. Fig. 9 represents the local Nusselt number distribution along one wave. The Nusselt number increases in the location of the recirculation zone and reaches a maximum at the reattachment point where renewal is accentuated. In this point, the particular local flow is of benefit to the heat transfer. This increase is available during the reverse flow region.

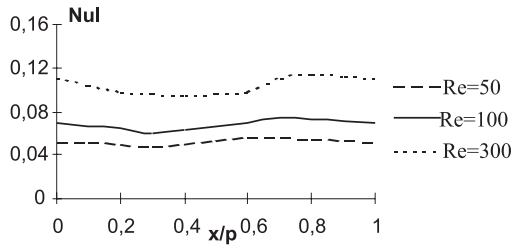


Fig. 9. Local Nusselt number distributions.

From the reattachment point, the local Nusselt number decreases until the next separation point. The maximum of the local Nusselt number shifts higher when the Reynolds number increases, due to the fact that the vortex is more intense. The increase in heat transfer at the wall for the case of the wavy wall is a consequence of benefiting from hydrodynamic conditions at the place of the recirculation and at the reattachment point.

In Fig. 10, a comparison between the mean Sherwood number on one wave is represented. The comparison is made for the same projected area. The mean Sherwood number is enhanced in this Reynolds flow range. The increase is not as important as in the case of heat transfer. If the comparison is established for the same tube area the enhancement still exists, but is less important. An explanation may be that the recirculation zone located in the furrow, does not exceed 70% of the total thickness of the film, hence the interface is not affected by this recirculation zone. Therefore, the vortex does not renew the concentration boundary layer at the interface and the characteristics of the mass transfer are the same as the case of a falling film flowing over a smooth tube. Moreover, the film becomes thicker on the recirculation zone so the mass transfer boundary layer is more important. As a consequence the resistance to the mass transfer increases.

Simulations with mass transfer alone (without heat transfer) show that the mean Sherwood number has a lesser increase than in the case of the simultaneous heat and mass transfer. Therefore, much of the increase in the mean Sherwood number, for the wavy tube, is induced by the heat transfer enhancement.

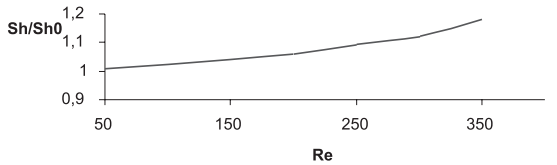


Fig. 10. Comparison of the global Sherwood numbers.

## 4. Conclusion

For the laminar flow range, the hydrodynamics, heat and mass transfer are numerically investigated for a falling film flowing inside a wavy walled tube. The surface shape induces a recirculation zone in the furrow of the waves. This recirculation zone grows up in size and in strength as the Reynolds number increases. The creation of the recirculation zone implies an increase in the film thickness. With the vortex there is a reversed flow near the wall. This flow creates a renewal of the thermal boundary layer at the wall which increases the heat transfer rate. For this range of Reynolds numbers the mass transfer is not directly affected by the recirculation zone. The vortex does not reach the interface, therefore the mass transfer rate is not greatly increased. The slight enhancement is due to both the increase in transfer area and to the heat transfer. In the results, the heat transfer undergoes a greater increase than the mass transfer. This is due to the fact that the Nusselt number is calculated at the wall where the recirculation zone is located and the Sherwood number is calculated at the interface which is not reached by the recirculation zone.

The turbulent flow regime is one of our preoccupations because in this regime, the vortex size and strength are more important and heat transfer is greatly affected. The vortex size is able to reach the interface and create the renewal of the concentration boundary layer, and therefore to increase mass transfer.

Another preoccupation is an experimental validation of the models. The experimental study is in process of being setup and it consists of the determination of the interfacial position. The experimental apparatus consists of a CCD video camera connected to an image treatment software package: OPTILAB.

## Appendix A. Newton method

Our problem is concerned with finding the solution of the non-linear system

$$\begin{aligned} &f_1(x_1, x_2 \ldots, x_n) = 0, \\ &\vdots \\ &f_n(x_1, x_2 \ldots, x_n) = 0 \end{aligned} \tag{24}$$

involving $n$ real functions and $n$ real variables. We define the following vectors:

$$x = (x_1, x_2 \ldots, x_n)^t,$$
$$F(x) = (f_1(x), f_2(x), \ldots, f_n(x))^t.$$

With the initial vector $x_0$, the method can be decomposed into four steps:

1. Initialisation.
2. Resolution of the linear system

$J(x^k)\,\mathrm{d}x^k = -F(x^k)$.

3. Calculation of $x$ for the next iteration

$x^{k+1} = x^k + \mathrm{d}x^k$.

4. Convergence test

If the test is satisfied $X^{k+1}$is the solution.

If the test is not satisfied go to step 2.

$J$ represents the Jacobian matrix. By a judicious arrangement, $J$ is a three-diagonal block matrix

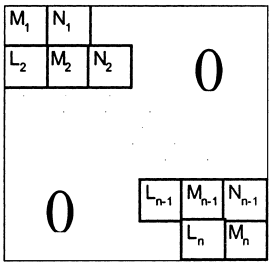


Each block $L_k$, $M_k$, $N_k$ represents a submatrix of the matrix $J$. $J$ has a sparce structure because a great majority of its terms are zeros.

## References

[1] T. Nishimura, Y. Ohory, Y. Kajimoto, Y. Kawamura, Mass transfer characteristics in a channel with symmetric wavy wall for steady flow, J. Chem. Eng. Jpn. 18 (1985) 550–555.

[2] T. Nishimura, Y. Ohory, Y. Kajimoto, Y. Kawamura, Flow characteristics in a channel with symmetric wavy wall for steady flow, J. Chem. Eng. Jpn. 17 (1984) 466–471.

[3] T. Nishimura, Y. Ohory, A. Tarumoto, Y. Kawamura, Flow structure and mass transfer for a wavy channel in transitional flow regime, J. Chem. Eng. Jpn. 19 (1986) 449–455.

[4] T. Nishimura, S. Murakami, S. Arakawa, Y. Kawamura, Flow observations and mass transfer characteristic in symmetrical wavy walled channels at moderate Reynolds numbers for steady flow, Int. J. Heat Mass Transfer 33 (1990) 835–845.

[5] E.M. Sparrow, J.W. Comb, Effect of interwall spacing and fluid flow inlet conditions on a corrugated wall heat exchanger, Int. J. Heat Mass Transfer 26 (1983) 993–1005.

[6] E.M. Sparrow, L.M. Hossfeld, Effect of rounding of protruding edges on heat transfer and pressure drop in a duct, Int. J. Heat Mass Transfer 27 (1984) 1715–1723.

[7] M. Molki, C.M. Yuen, Effect of interwall spacing on heat transfer and pressure drop in a corrugated wall duct, Int. J. Heat Mass Transfer 29 (1986) 987–997.

[8] Y. Asako, H. Nakamura, M. Faghri, Heat transfer and pressure drop characteristics in a corrugated duct with rounded corners, Int. J. Heat Mass Transfer 31 (1988) 1237–1245.

[9] G. Rub, H. Beer, Heat transfer augmentation due to turbulence promotion in a pipe with sinusoidal wavy surface, in: Heat transfer 1984, Proceedings of the 10th International Conference of Heat Transfer, 1994, pp. 315–320.

[10] G. Tanda, G. Vittori, Fluid flow and heat transfer in a two-dimensional wavy channel, Heat Mass Transfer 31 (1996) 411–418.

[11] N. Siniei, S. Dini, Heat transfer characteristics in a wavy-walled channel, J. Heat Transfer 115 (1993) 788–792.

[12] R.C. Xin, Q. Tao, Numerical prediction of laminar flow and heat transfer in wavy channels of uniform cross-sectional area, Numer. Heat Transfer 14 (1988) 465–481.

[13] J.C. Slattery, Interfacial Transport Phenomena, Springer, New York, 1990.

[14] R.C. Reid, J.M. Prausnitz, T.K. Sherwood, The Properties of Gases and Liquids, third ed., McGraw-Hill, NewYork, 1977.

[15] R.C. Reid, J.M. Prausnitz, B.E. Poling, The Properties of Gases and Liquids, fourth ed., McGraw-Hill, New York, 1987.

[16] J.E. Vivian, C.J. King, Diffusivities of slightly soluble gases in water, AIChE J. 10 (1964) 220–221.

[17] D.R. Olander, The diffusivity of water in organic solvents, AIChE J. 7 (1961) 175–176.

[18] F.P. Lees, P. Sarram, Diffusion coefficient of water in some organic liquids, J. Chem. Eng. Data 16 (1971) 41–44.

[19] Prophy, Notice technique, Toulouse, 1993.

[20] P.K. Panday, Laminar film condensation of turbulent vapour flowing inside a vertical tube, in: Proceedings of the Second International Symposium on Condensers and Condensation, University of Bath, UK, 28–30 March 1990, pp. 473–482.

[21] S. Negny, M. Meyer, M. Prevost, Simulation of velocity fields in a falling film with a free interface flowing over a wavy surface, Comput. Chem. Eng. 22 (1998) S921–S924.

[22] I.J. Sobey, On flow through furrowed channels – Part 1 calculated flow patterns, J. Fluid Mech. 96 (1980) 1–26.

[23] S.M. Yih, K.Y. Chen, Gas absorption into wavy and turbulent falling liquid film in a wetted-wall column, Chem. Eng. Com. 17 (1982) 123–136.